(27)

COMPUTATION OF NONLINEAR WAVE KINEMATICS DURING PROPAGATION AND RUNUP ON A SLOPE

S. GRILLI and I.A. SVENDSEN
Ocean Engineering Program, Department of Civil Engineering
University of Delaware
Newark-DE 19716, USA

ABSTRACT. An efficient Boundary Element Method (BEM) solving fully nonlinear waterwave problems in the physical space has been developed in our earlier papers. Its detailed numerical features have been presented elsewhere. In the present paper, this method is applied to the computation of the interaction between highly nonlinear solitary waves and plane steep and gentle slopes. Kinematics of the waves is calculated during propagation and runup on a slope. In particular, the internal velocity field above the slope and the pressure force on the slope are computed in detail during runup and rundown of the wave. The results show features of the wave flow such as jet-like up-rush, stagnation point and breaking during backwash. A comparison is made with accurate experimental results (runup, surface elevations), with orther fully nonlinear solutions, and also with the predictions of the Shallow Water Wave Equation. The results show that the BEM used here is capable of accurately describing the wave flow and interaction with a plane slope(2.88° to 90°), in great detail.

1 Introduction

1.1 Numerical modelling of nonlinear water waves

Over the last decade numerical solution of the exact nonlinear equations for water waves, using a Boundary Integral Equation (BIE) description, has become an increasingly successful method. In particular, one of the most impressive achievements of this method was the modelling of overturning waves (plunging breaker). Practically all previous contributions, however, utilized space periodicity of the waves and most of them also were based on a conformal mapping of physical space onto a plane in which the equivalent of the free surface was the only part left of the boundary (the BIE was then solved in the transformed plane). A few contributions used some other complex variable-dependent techniques. There are many advantages of this method which has been explored extensively by many authors. Particularly noteworthy for significant steps to the development are contributions by Longuet-Higgins & Cokelet 1976 [23], Vinje & Brevig 1981 [37] and Dold & Peregrine 1984 [7]. The procedure, however, also has some important limitations which are associated with the use of complex variables and with the assumption of waves that are periodic in space.

In our previous papers (Grilli, Skourup & Svendsen 1988, 1989 [14,15], Grilli & Svendsen 1989a,b [16,17]) we presented an equally efficient and accurate method, without utilizing

A. Tørum and O. T. Gudmestad (eds.), Water Wave Kinematics, 387–412.

those two crucial assumptions and we demonstrated its application to some problems for which the above-mentioned version is not well suited. In this two-dimensional model (2D), we considered the wave motion in the physical space and described it using a free space Green's function to transform the Laplace differential equation into an integral equation that involved only values of the velocity potential and its normal derivative along the physical boundary. Our procedure is a Boundary Element Method (BEM) developed for higher order elements. The time integration is an the explicit scheme correct to second order in Δt using the shape functions of the BEM.

1.2 Interaction of nonlinear waves with maritime structures

An accurate theoretical prediction of the interaction of real waves with maritime structures is essential for the study of coastal protection. These structures have very often their main dimension in the long-shore direction and can be analyzed quite accurately by 2D models in their cross-section (Figure 1a) which can reasonably be represented by a steep plane slope, or a combination of plane slopes and berms. The sea bottom in the shallow water area in front of such a structure can itself be approximated by a gentle plane slope on which the very high waves (e.g. greater than 0.7 times the water depth) will break without any significant reflection, before reaching the structure (Figure 1a, wave (a)).

The numerical modelling of the interaction of waves with a maritime structure aims at determining the maximum and minimum vertical elevations of the waves during their reflection on the structure (runup and rundown), the reflected wave characteristics (phase shift, reflection coefficient), and the pressure distribution on and wave particle velocity close to the slope (essential for the estimation of local and global stability of the structure and of its elements); finally the prediction of the breaking of waves during runup and backwash provides important data for determining local reinforcements of the structure. The numerical modelling of the interaction between very high waves and gentle slopes in front of maritime structures will concentrate on the shoaling and breaking processes. Notice, however, that a gentle slope can also be the approximation of a beach, which makes it interesting to also studying with the model non-breaking runups of smaller waves on gentle slopes.

Although the model can generate and propagate fully nonlinear waves in a two-dimensional physical space, it cannot yet simulate the interaction with a structure of long time series of periodic waves, like they occur in nature. Waves are generated in the model by simulating a wavemaker at one end of a numerical wave tank and are propagated toward a structure modelled at the other end of the tank. After interacting with the structure, partially reflected waves propagate back in the tank, toward the wavemaker, where they reflect again, and so on. From that time onward, these waves interact with other waves generated in the tank, which soon leads to the development in the model of partially standing waves. This reflection from the wavemaker, also essentially occurs in a physical tank and prevents us from running long term numerical experiments with periodic waves.

Moreover, though this kind of model is capable of modelling overturning waves, the computations break down when the tip of the *first* breaking wave hits the free surface. Thus, even if we were able to model long time series of waves, breaking would constitute an important limitation for using such a model for design purposes.

A solitary wave, however
wave on a slope is the reflectio
made before the wave propag
wave propagation and interac
present version of our model.
a *Tsunami* and, as pointed out
the most massive waves, and h
structures can thus be used as

Hence, in the present pap
between solitary waves and pla
runup, breaking and reflection
capable of quite accurately des
time. After briefly describing
wave by a "numerical wavema
waves with steep slopes is pres

2 General features

In the present form of the two-
physical space $\Omega(t)$ (Figure 1b
for a 2D irrotational inviscid fl
using the free space Green's
equation into an integral equa
its normal derivative along the

$$\alpha(\mathbf{x}_l)\phi(\mathbf{x}_l) = \int_\Gamma [\frac{\partial \phi}{\partial n}(\mathbf{x})G$$

where $\mathbf{x} = (x, z)$ and $\mathbf{x}_l = (x_l,$
is a geometric coefficient.

In our BEM, collocation
the variation of boundary geo
tions of the problem. Betwe
described by means of shape f
elled by cubic splines and fie
the boundary is divided into e
of the computations reported
used). Mapping onto isopara
mapping function is determine
sian quadrature, and a kernel
then computed by a Gauss-lik

The nonlinear kinemati
surface $\Gamma_f(t)$. Solitary waves
on the boundary $\Gamma_{r1}(t)$ and b
stationary bottom Γ_b and the

A solitary wave, however, does not pose the same problem. The reflection of a solitary wave on a slope is the reflection of *one* well defined wave only whose detailed study can be made before the wave propagates back to the wavemaker and interacts with it. Solitary wave propagation and interaction with structures can thus well be simulated with the present version of our model. Furthermore solitary waves ressemble the waves generated in a *Tsunami* and, as pointed out by Fenton & Rienecker 1982 [9], they are also the fastest and the most massive waves, and have the greatest impulse. Their pressure forces on maritime structures can thus be used as design criteria.

Hence, in the present paper, we apply the model to the computation of the interaction between solitary waves and plane slopes (both steep and gentle). Generation, propagation, runup, breaking and reflection of the waves are studied in detail and show that our BEM is capable of quite accurately describing the flow in great detail and over extensive periods of time. After briefly describing the model features in Section 2, the generation of a solitary wave by a "numerical wavemaker" is presented in Section 3. The interaction of solitary waves with steep slopes is presented in Section 4 and with gentle slopes in Section 5.

2 General features of the model

In the present form of the two-dimensional model, nonlinear wave problems are solved in the physical space $\Omega(t)$ (Figure 1b). The solution of the Laplace problems (continuity equation for a 2D irrotational inviscid fluid) is based on a non-complex method : a high order BEM, using the free space Green's function $G(\mathbf{x},\mathbf{x}_l)$ which transforms the Laplace differential equation into an integral equation that involves only values of the velocity potential and its normal derivative along the physical boundary $\Gamma(t)$,

$$\alpha(\mathbf{x}_l)\phi(\mathbf{x}_l) = \int_\Gamma [\frac{\partial \phi}{\partial n}(\mathbf{x})G(\mathbf{x},\mathbf{x}_l) - \phi(\mathbf{x})\frac{\partial G(\mathbf{x},\mathbf{x}_l)}{\partial n}]\, d\Gamma \qquad (1)$$

where $\mathbf{x} = (x,z)$ and $\mathbf{x}_l = (x_l,z_l)$ are position vectors for points on the boundary, and $\alpha(\mathbf{x}_l)$ is a geometric coefficient.

In our BEM, collocation nodes are distributed along the entire boundary to describe the variation of boundary geometry as well as boundary conditions and the unknown functions of the problem. Between the collocation points, the variation of all quantities is described by means of shape functions (linear to quartic) or quasi-splines (geometry modelled by cubic splines and field variables by linear shape functions). For this purpose, the boundary is divided into elements each of which contains two or more nodes (in most of the computations reported hereafter, quadratic and quasi-spline elements have been used). Mapping onto isoparametric reference elements is used and the Jacobian of the mapping function is determined analytically. The regular integrals are computed by Gaussian quadrature, and a kernel transformation is applied to the singular integrals which are then computed by a Gauss-like quadrature weighted with a logarithmic singularity.

The nonlinear kinematic and dynamic boundary conditions are imposed on the free surface $\Gamma_f(t)$. Solitary waves are generated by simulating a piston-type wavemaker motion on the boundary $\Gamma_{r1}(t)$ and by imposing the continuity of its normal velocity. Along the stationary bottom Γ_b and the slope Γ_{r2}, a zero normal velocity is imposed.

The time integration of the free surface conditions is the explicit scheme developed by Grilli, *et al.* 1989 [15]. It is based on a truncated Taylor expansion (Dold & Peregrine 1984 [7]) which has been modified to using the shape functions or the quasi-splines of the BEM. A version correct to second order in Δt ($n = 2$) has been developed for the computations presented here. The updating of the free surface position r from time t to $t + \Delta t$ reads,

$$\mathbf{r}(t+\Delta t) = \mathbf{r}(t) + \sum_{k=1}^{n} \frac{(\Delta t)^k}{k!} \frac{D^k \mathbf{r}(t)}{Dt^k} + O[(\Delta t)^{n+1}] \qquad \text{on } \Gamma_f(t) \tag{2}$$

and the analogous for ϕ.

To get the coefficients in the expansions, we solve a succesion of Laplace problems (two in our case) for the velocity potential and its time derivatives, each problem solution providing the nonlinear free surface boundary conditions for the next one. The expansion coefficients are expressed in terms of ϕ, $\frac{\partial \phi}{\partial n}$, $\frac{\partial \phi}{\partial t}$ and $\frac{\partial^2 \phi}{\partial t \partial n}$ and their derivatives along the free surface. We adopt a coordinate system at the free surface defined by (s,n), the tangential and normal unit vectors to the free surface. This formulation provides simpler expressions for the high order derivatives than a cartesian system. For the evaluation of the derivatives along the free surface we use a sliding 4th order polynomial element independant of the BEM discretization. It provides a local continuity on the boundary of at least the 2nd derivatives.

The overall stability of the method has permitted us so far to avoid smoothing procedures. Notice that all the present features of this 2-D model can in principle be extended to 3-D problems.

A detailed account of the 2D-BEM applied to our water wave problem is given in Grilli, Skourup & Svendsen 1989 [15].

3 Wave generation by a wavemaker

3.1 Generation of a first order solitary wave

The model described above (Section 2) can propagate waves in space and time. Since the computations are made in physical space, however , and only cover a limited region of an infinitely long wave tank, the waves to be studied have to be generated at the outer edge of the computational area. Waves will be generated in this study by simulating a wavemaker movement. Other methods exist, however, for generating waves without moving any body (see e.g. Grilli, *et al.* 1988, 1989 [14,15], Grilli & Svendsen 1989 [16]).

The generation of waves by a numerical wavemaker requires the movement of one of the tank boundaries on a way it creates the desired wave. In many experimental studies (Goring 1978 [11], Losada, *et al.* 1986 [24]) and numerical computations (Kim, *et al.* 1983 [20]), the waves were generated by a piston motion wavemaker (physical or numerical) which was moved to create a *first-order* solitary wave according to Goring's method. This type of generation has been reproduced here as closely as possible (see Appendix A for detail).

Within the frame of Boussinesq approximation, the inverse scattering theory (Gardner, *et al.* 1967 [10], Hammack & Segur 1974 [19]) will predict that, unless it corresponds to an exact solitary wave, a distributed elevation of the free surface will disintegrate into one or more solitons and a tail of disturbances. Thus, a *first-order* solitary wave of appreciable

height generated in the model n
its profile while it propagates d
limit for an accurate solitary wa
with this, it is found that the
the tail of disturbances they ar

3.2 Free surface intersec

If the waves are generated by s
a corner on the boundary curv
situation appears when dealing

The flow near such inters
rise to substantial concern in t
linear waves, the intersection wi
between the flow requirements
wall. Kravtchenko's derivation
the wall. This was in fact furth
impulsively accelerated wall, an
of Greenhow & Lin 1986 [13].

In a more detailed investig
acceleration remains bounded,
not particularly smoothly behav
neglected, as Peregrine does, ev
under certain constraints, limit t
He also found that away from t
order, as verified by Greenhow
remains finite (even the dramat
not mathematically an impulsiv
al. 1988 [6].

In conclusion the existence
haunting many investigators usi
for the fully nonlinear case. In o
cient care is exercised during th
acceleration).

It should be noticed that ev
is proved to be singular close t
problem can only provide results
representing this solution. In the
on the free surface by a piecewise
functions within each boundary
never become anything but a po
will never be approximately rep
If the corner singularity of the so
substitute the appropriate singu
to the corner. This technique, s

height generated in the model may be expected to exhibit disturbances and modifications of its profile while it propagates down the wave tank. In fact Goring 1978 [11] found that the limit for an accurate solitary wave reproduction by his method was $\frac{H}{d} = 0.2$. In accordance with this, it is found that the higher the waves, the more pronounced is the amplitude of the tail of disturbances they are shedding (see Section 4.2).

3.2 Free surface intersection with moving bodies

If the waves are generated by simulating a wavemaker or a body movement, there will be a corner on the boundary curve where body surface and free surface meet and the same situation appears when dealing with the intersection with other surface piercing structures.

The flow near such intersections between a free surface and a solid body has given rise to substantial concern in the literature since Kravtchenko 1954 [21] showed that for linear waves, the intersection with a moving wall would generally create an incompatibility between the flow requirements of the boundary conditions along the free surface and the wall. Kravtchenko's derivations indicated that a logarithmic singularity would result at the wall. This was in fact further substantiated by Peregrine 1972 [29] for the case of an impulsively accelerated wall, and his findings seemed to be confirmed by the experiments of Greenhow & Lin 1986 [13].

In a more detailed investigation of the linear case, Roberts 1987 [30] found that if the acceleration remains bounded, the amplitude at the wall will also be bounded (although not particularly smoothly behaved) and that over a small but finite time gravity cannot be neglected, as Peregrine does, even with an impulsive start. Roberts found that this does, under certain constraints, limit the free surface elevation to finite values at the moving wall. He also found that away from the wall the free surface variation *is* logarithmic to leading order, as verified by Greenhow & Lin's experiments, even when the amplitude at the wall remains finite (even the dramatic acceleration they produced by a sledge hammer is still not mathematically an impulsive start). This problem has also been studied by Cointe, et al. 1988 [6].

In conclusion the existence at the corner of the logarithmic singularity that has been haunting many investigators using the BIEM or BEM, has still to be proved theoretically for the fully nonlinear case. In our model it does not seem to be a problem provided sufficient care is exercised during the first few time steps starting the computations (bounded acceleration).

It should be noticed that even if the actual mathematical solution of the flow equations is proved to be singular close to the corner, the approximate numerical solution of the problem can only provide results according to the functions used in the numerical model for representing this solution. In the case of the BEM, for instance, if the potential is modelled on the free surface by a piecewise polynomial approximation of unknown magnitude (shape functions within each boundary element), the numerical solution close to the corner will never become anything but a polynomial variation. In particular, a logarithmic variation will never be approximately represented in the results (as observed in our computations). If the corner singularity of the solution can be identified mathematically, however, one can substitute the appropriate singular function (whatever it is) in the numerical model close to the corner. This technique, sometimes named "singular shape function" has been very

succesful in such fields as fracture mechanics. To apply here, it would require to determine the leading order of the solution in the corner for the fully nonlinear case.

Care must also be taken to ensure the well-posedness of the flow equations and boundary conditions to be solved by the numerical method. Numerical singularity can occur in the BEM, for instance, if one does not take into account that both the potential and its normal gradient are known on the body part of the corner. Therefore we use double nodes at the corners (providing two different normal directions and unknowns on the two sides of each corner) and we include the relations between the ϕ's and the $\frac{\partial \phi}{\partial n}$'s at the corner points, in the BEM system, as compatibility conditions (for detail see Grilli, *et al.* 1988, 1989 [14,15]). Lin, Newman & Yue 1984 [22] handled the corner problem by specifying both the potential and the stream function at the body part of the corner in their Cauchy integral theorem formulation. Doing so, they could generate nonlinear waves by a wavemaker. Using a similar technique, Greenhow & Lin 1985 [12] and Yim 1985 [38] simulated nonlinear wedge entries in water. Dommermuth & Yue 1987 [8], following the same principle as Lin, et al., imposed both the potential and its normal derivative at the body part of the corner in their BEM formulation. Since these methods seem to work, it is assumed that they treat the corner problem in a way similar to the method we use in our model, although the authors do not give details.

4 Interaction of a solitary wave with a steep slope

4.1 Background

Runup and reflection from plane slopes of non-breaking solitary waves have been studied quite extensively in the literature. In fact, the solitary wave runup problem using the exact equations was studied numerically already by Camfield & Street 1967 [3] by means of a marker and cell method. More commonly, however, the runup of solitary waves has been analyzed using long wave theory or Boussinesq theory. The special case of reflection from a vertical wall is equivalent to the problem of collision between two opposing solitary waves of the same height and several studies have been published utilizing that analogy. A first order solution was obtained by the Inverse Scattering Technique developed in the 1960's and 70's (Gardner,*et al.* 1967 [10]), and a third order analysis was developed by Su & Gardner 1969 [33] and Su & Mirie 1980 [32] and solved numerically by Mirie & Su 1982 [25]. Higher order analysis were also done recently by Byatt-Smith 1988 [2]. Fenton & Rienecker 1982 [9] used a Fourier Method to obtain very accurate results for the same problem.

The runup on a slope was analyzed numerically on the basis of the Boussinesq equations by Pedersen & Gjevik 1983 [28], by a low order BEM by Kim, *et al.* 1983 [20] and Synolakis 1987 [35], using the SW equation, generalized the approach of Carrier 1966 [4] to apply to the situation also considered in this paper with a constant depth region in front of the slope.

Notice that the method we have developed here makes it possible to model any kind of bottom or slope geometry, like obstacles of arbitrary shape, shelf or combination of slopes and berms as long as flow separation is not important.

4.2 Generation and prop

Since our numerical computatio
should be expected closely to foll
ation of the wave motion. Figur
$\frac{H}{d}$, generated by a piston wavem
of depth $d = 0.3$m, at the (differ
m in front of the wave generator
found that the higher the waves
the tail of disturbances they are
the highest parts of the crests a
between front and rear for the lo

As the waves propagate fu
creases and the part of the tail cl
3 shows this in a comparison be
ing propagated only 6m (20 d)
transformation of the wave profil
results in a moderate decrease in

4.3 Reflection from a ver

Before considering the reflection
vertical wall. In Figure 4, the ma
different wave amplitudes is com
obtained for that situation using
& Mirie 1980 [32] (S&M). The
results of the BEM fall a little b
the incoming wave is not quite a
(different number of nodes N_Γ a
136 or 158, Δt= 0.0075 to 0.020s

If we analyze the mass an
we find that for most of the pro
0.01 %. In the brief interval of th
energy increases by about 0.06 %
t shows that, in this case, each
volume. This suggests that the r
of the process where the surface
(fixed) time step used in the com
predicted with quite the same ac

Figure 5 shows the kinetic
kinetic energy has its minimum a
zero. In spite of the increase in
there is a slight decrease in kinet
further substantiated by the anal

F&R also compute total ma
view of the close agreement descri

4.2 Generation and propagation

Since our numerical computations solve the full nonlinear equations, the computed waves should be expected closely to follow what actually happens in a wave flume after the generation of the wave motion. Figure 2 shows profiles of waves with seven different amplitudes $\frac{H}{d}$, generated by a piston wavemaker (according to Goring's first order solution) in a tank of depth $d = 0.3$m, at the (different) time when the crest of each of them passes a point 6 m in front of the wave generator. In accordance with the comments above (Section 3), it is found that the higher the waves, the more pronounced is the amplitude A (Figure 1b) of the tail of disturbances they are shedding. A closer inspection also shows that, although the highest parts of the crests are closely symmetric, there are non-negligeable differences between front and rear for the lowest 25-35 % of each profile.

As the waves propagate further away from the wave generator, the asymmetry decreases and the part of the tail closest to the wave turns into a long, shallow trough. Figure 3 shows this in a comparison between two waves of the same height ($\frac{H}{d}$= 0.257), one having propagated only 6m (20 d) since generated, the other after 26m (86.7 d). The slow transformation of the wave profile as it propagates and adjusts itself to a stable form, also results in a moderate decrease in wave height.

4.3 Reflection from a vertical wall

Before considering the reflection from a slope, we analyze the more simple reflection from a vertical wall. In Figure 4, the maximum elevation ("runup", R_u) at the wall computed for different wave amplitudes is compared to the results of Fenton & Rienecker 1982 [9] (F&R) obtained for that situation using a Fourier Method, and to the third order results by Su & Mirie 1980 [32] (S&M). The general impression is that for amplitudes above 0.3, the results of the BEM fall a little below the other two methods. Part of this can be because the incoming wave is not quite a solitary wave, part could be computational inaccuracies (different number of nodes N_Γ and time steps Δt were used in the computations : N_Γ= 136 or 158, Δt= 0.0075 to 0.020s).

If we analyze the mass and energy balance of the system for a wave of $\frac{H}{d}$=0.456, we find that for most of the propagation, the total energy E_T remains constant to within 0.01 %. In the brief interval of the rapid surface movements at the wall, however, the total energy increases by about 0.06 %. A detailed analysis of the volume error as a function of t shows that, in this case, each change in total energy is matched by a similar change in volume. This suggests that the reason for the energy gain is that during the short interval of the process where the surface is moving really fast up and down along the wall, the (fixed) time step used in the computations is too large, so that the surface movement is not predicted with quite the same accuracy during that part of the process.

Figure 5 shows the kinetic energy E_K during the BEM computations. One sees the kinetic energy has its minimum a fraction of a second before runup and never becomes quite zero. In spite of the increase in total energy during reflection, refered to above, one finds there is a slight decrease in kinetic energy (of 0.288 % in this case). These phenomena are further substantiated by the analysis of the velocity field made in Section 4.5.

F&R also compute total maximum forces and moments of forces acting on the wall, In view of the close agreement described above, it is not surprising that our BEM computations

$\frac{H}{d}$	N_Γ	$N_{\Gamma f}$	$\frac{\Delta x}{d}$	Δt(s)	CPU (s)
0.269	136	81	0.42	0.015	0.745
0.269	378	241	0.42	0.015	5.041
0.457	158	101	0.33	0.010	0.925

Table 1: Discretization and computation time for the BEM computations. $N_{\Gamma f}$ is the number of nodes on the free surface and $\frac{\Delta x}{d}$ represents the distance between 2 nodes on the free surface

β	$\frac{H_i}{d}$	$\frac{H_r}{d}$	K_r	$\frac{R_u}{d}$	$\frac{R_d}{d}$
90°	0.255	0.245	0.963	0.545	0.012
90°	0.456	0.416	0.913	1.071	0.056
70°	0.259	0.243	0.937	0.580	0.014
70°	0.437	0.378	0.866	1.062	0.096
45°	0.269	0.222	0.825	0.674	0.137
45°	0.457	0.358	0.785	1.257	0.386

Table 2: BEM computations : Solitary wave on a slope β. $\frac{H_i}{d}$ corresponds to the incident wave at $x = 6$m and $\frac{H_r}{d}$ to the reflected wave at the same location. $\frac{R_u}{d}$ and $\frac{R_d}{d}$ are the runup and rundown of the wave. $K_r = \frac{H_r}{H_i}$ is the reflection coefficient.

give results that coincide to a fraction of a percent for these quantities (Figure 6). A somewhat surprising result is a double maximum found in the time variation of the total force for high waves (Figure 7). A wave of $\frac{H}{d} = \varepsilon = 0.4$ already shows sign of an extended maximum and for $\varepsilon = 0.5$ and 0.6, there is distinctively two extremes on the force curve 0.2-0.3s apart. In the case of $\varepsilon = 0.6$, the computations broke down at the time of the second maximum in a situation with essentially zero pressure and a free falling water volume near the crest. Such a double maximum of the wave force in a fairly short time constitutes a very strong loading for maritime structures. It may be noticed that experiments of the runup of steep periodic waves on a vertical wall, made by Nagai 1969 [26], showed somewhat similar features.

4.4 Reflection from a steep slope

Numerical experiments have been made for the cases of slope angles $\beta = 45°$, 70° and 90° to compare with the laboratory experiments made by Losada, *et al.* 1986 [24] (LVN). Our numerical wave tank was 10m long and 0.3m deep. Key figures for the computations presented in the following are given in Table 1 (discretization and computation times on an IBM 3090/200) and in Table 2 (wave data, reflected wave, runup and rundown). Due to the vectorization of the computations, the CPU-time per time step was found to increase less than proportional to the square of the number of nodes as indicated by the figures in

β	$\frac{H}{d}$
90°	0.
90°	0.
70°	0.
70°	0.
45°	0.
45°	0.

Table 3: Experimental results
Table 2).

Table 1 (378 nodes) for the com
The experimental results are gi

As mentioned in Section
33 water depths from the slope
is adjusted here, so that when t
0.259, 0.269 or 0.456, 0.437, 0.
periments. The comparison bet
results of Table 3 shows a close
of the waves and a reasonable a
and reflection coefficients $K_r =$

Figures 8 and 9 show son
and $\frac{H}{d} = 0.457$. Figure 8 sho
to maximum runup on the slo
(the wave propagates leftward),
distance away from the slope (
curve shown in Figure 9. Notic
the description of this breaking
in its present form, and this n
somewhat similar breaking patt
to that particular wave.

Figures 10 and 11a-b pres
surface elevations and those me
results have been synchronized
reported, is the only well-define
temporal development is genera
of the wave, however, at that t
which preceed the runup as de
with the experimental results is
so also for the preceeding part

Figure 10 shows how a wa
are compared with the measure
is the instant of maximum run

β	$\frac{H_i}{d}$	$\frac{H_r}{d}$	K_r	$\frac{R_m}{d}$	$\frac{R_d}{d}$
90°	0.255	0.224	0.882	0.521	0.003
90°	0.456	0.419	0.918	1.107	0.059
70°	0.259	0.232	0.893	0.558	0.001
70°	0.437	0.423	0.968	1.071	0.113
45°	0.269	0.214	0.796	0.672	0.129
45°	0.457	0.347	0.759	1.294	0.267

Table 3: Experimental results from Losada *et al.* 1986 : Solitary wave on a slope β (see Table 2).

Table 1 (378 nodes) for the computations with the long wave tank (30m) mentioned above. The experimental results are given in Table 3.

As mentioned in Section 3, in the computations, we generate the wave at $x = 0$ (i.e., 33 water depths from the slope) by Goring's procedure. The amplitude of the wavemaker is adjusted here, so that when the wave passes $x = 6$m (20 d), it has a height of $\frac{H_i}{d}$=0.255, 0.259, 0.269 or 0.456, 0.437, 0.457 which corresponds to those used by LVN in their experiments. The comparison between the numerical results of Table 2 and the experimental results of Table 3 shows a close agreement between the values of the maximum runups $\frac{R_m}{d}$ of the waves and a reasonable agreement between the values of the maximum rundowns $\frac{R_d}{d}$ and reflection coefficients $K_r = \frac{H_r}{H_i}$.

Figures 8 and 9 show some free surface elevations computed for the case of $\beta = 45°$ and $\frac{H_i}{d} = 0.457$. Figure 8 shows the incoming solitary wave propagating rightward, up to maximum runup on the slope. Figure 9 shows phases of the rush-down on the slope (the wave propagates leftward), with the development of a backward breaking, at a small distance away from the slope ($x \simeq 9.8$m). The computations broke down after the last curve shown in Figure 9. Notice that very few nodes in the computations are involved in the description of this breaking phenomenon. Clearly we reach the limits of our 2D-model in its present form, and this needs to be investigated further. Notice, however, that a somewhat similar breaking pattern was observed by LVN in the experiment corresponding to that particular wave.

Figures 10 and 11a-b present some detailed comparisons between our computed free surface elevations and those measured by LVN. In all cases, the computed and measured results have been synchronized at the time of maximum runup which, in the experiments reported, is the only well-defined time available. That means that actual comparison of the temporal development is generally limited to the time after the maximum runup. The form of the wave, however, at that time follows entirely from the generation and propagation which preceed the runup as described in the previous Section. And since the agreement with the experimental results is so good after that time, it is anticipated that it would be so also for the preceeding part of the process.

Figure 10 shows how a wave of $\frac{H_i}{d}$=0.269 reflects from a 45° slope. The computations are compared with the measured surface profiles at three different times, of which the first is the instant of maximum runup. Since the computed time of the lowest position of the

water surface at the slope does not quite coincide with the time of the measured minimum, we have shown both. The symbols mark data points that have been developed from the original experimental records with the kind assistance of Dr. Losada, and the dotted curve is a spline fit to these points. In general, the agreement is considered good. Figure 11a shows the results for a wave of $\frac{H}{d}$=0.437, on a 70° slope. Here an extra profile (a) is available before the wave reaches the slope. As in the first case, the agreement between physical and numerical experiments is surprisingly good. Notice that even the irregularities left after the main crest has cleared the slope are quite well represented. Figure 11b further confirms this, by showing detail of the "wave tail" at an even later time. The agreement is still good, even for such small scale oscillations. This attests to the care exercised in the experiments and to the accuracy of the computational technique. The very small oscillations of the order of 1mm left behind the wave for $x \geq$8.5m are mainly *numerical noise*. One obviously reachs here the limits of the resolution one can expect from the discretization used in this problem.

4.5 The internal velocity field during runup and rundown

The examples in the previous Section show that it is possible to reproduce surface variations recorded in experiments down to very small details and over quite extended periods of time relative to the time scale of the important events. This can only be possible if the computational solution actually represents the whole flow pattern to a high degree of accuracy. Thus it is possible to use the computational solution to analyze other properties of the flow (like the internal velocity) than those actually measured in the experiments and to have a reasonable confidence in the correctness of such predictions.

The numerical procedure that computes the development of the wave motion in space and time in our model, leaves us with both the velocity potential ϕ and $\frac{\partial\phi}{\partial n}$, known at all time steps (see Grilli 1988, 1989 *et al.* [14,15]). Therefore, the computation of the velocity at an internal point is a theoretically straight-forward evaluation of an integral. At an internal point $\mathbf{x}_o = (x_o, z_o)$, the velocity potential is given by (1) with $\alpha(\mathbf{x}_o)$=1. Differenciation of this expression with respect to x_o and z_o yields the velocity components (u, v),

$$u(\mathbf{x}_o) = \int_\Gamma [\frac{\partial\phi}{\partial n}(\mathbf{x})\frac{\partial G(\mathbf{x},\mathbf{x}_o)}{\partial x_o} - \phi(\mathbf{x})\frac{\partial^2 G(\mathbf{x},\mathbf{x}_o)}{\partial n \partial x_o}]\, d\Gamma \tag{3}$$

$$w(\mathbf{x}_o) = \int_\Gamma [\frac{\partial\phi}{\partial n}(\mathbf{x})\frac{\partial G(\mathbf{x},\mathbf{x}_o)}{\partial z_o} - \phi(\mathbf{x})\frac{\partial^2 G(\mathbf{x},\mathbf{x}_o)}{\partial n \partial z_o}]\, d\Gamma \tag{4}$$

These integrations can be performed by Gaussian quadrature, since they are regular as long as the observation point $\mathbf{x}_o$ stays inside the domain.

We have computed the internal velocity field at some points in the neighborhood and above a 45° slope, during runup and rundown of a solitary wave of $\frac{H}{d} = 0.457$. To measure velocities in that detail in the physical experiments would be a tremendous task, whereas it only requires a limited extra effort computationally. This illustrates the usefulness of combining experiments and numerical computations.

Figure 12a-d shows the velocity field at four different stages . When the first part of the wave reaches the slope, the flow field looks almost like a rotation around a point well above the incoming wave crest. Then, as the wave crest approaches the slope, the upward

movement almost looks like a
there is still a jet-like up-rush o
near the toe of the slope as a
stagnation point moves up along
in the combination of high velo
position. The steep shoreward s
horizontal accelerations close t
directed pressure gradient which
slope. The damage to rubble mo
occurs at this stage of the proce
breaking already mentioned bef

4.6 Pressure on the slop

One of the questions that can b
wave runup is: How well will
describe this flow. Those equati
for periodic waves on a steep s
[35]. It is of interest to know to
flow situation as computed here

It is well known that in t
hydrostatic and, on a horizontal
uniform over the entire depth. E
to apply on a steep slope. There
computed here deviates from th
one can expect from the much s

It is rather evident from
the large horizontal velocities a
order of magnitude. Therefore,
nonhydrostatic pressure which
uniform over depth. The pressu
by the hydrostatic pressure corr
the considered point at the slope.
from +1 (corresponding to an h
the runup phase the ratio stays w
between 0.6 and 1.9. The horiz
Figure 12. This leads to diagram
is almost invariably close to bei

The comparison with the
Grilli 1989 [33] and in the next

movement almost looks like a jet rushing up along the slope (Fig. 12a). In Fig. 12b, there is still a jet-like up-rush of the tip of the wave, but a stagnation point has developed near the toe of the slope as an indication of the reflection taking effect. Later on, this stagnation point moves up along the slope. Fig. 12c shows a remarkably interesting feature in the combination of high velocities and large accelerations around the time of the lowest position. The steep shoreward slope of the free surface in this non-distorted figure suggests horizontal accelerations close to 1 g. In a porous slope, there would be a strong outward directed pressure gradient which would result in a high risk of units being pulled out of the slope. The damage to rubble mound structures observed during experiments actually often occurs at this stage of the process. Finally, Figure 12d shows the beginning of the bakward breaking already mentioned before.

4.6 Pressure on the slope. Comparison with the SWE

One of the questions that can be asked when looking at these results for highly nonlinear wave runup is: How well will the nonlinear shallow water (NSW) equations be able to describe this flow. Those equations are the basis for Carrier & Greenspan 1958 [6] solution for periodic waves on a steep slope and were used for a solitary wave by Synolakis 1987 [35]. It is of interest to know to which extent this simpler formulation describes the actual flow situation as computed here.

It is well known that in the NSW equations representation, the pressure is assumed hydrostatic and, on a horizontal bottom, it follows implicitly that horizontal velocities are uniform over the entire depth. Even with this hypothesis, the NSW equations can be shown to apply on a steep slope. Therefore, the extent to which the solution to the exact equations computed here deviates from those ideal assumptions may indicate the degree of accuracy one can expect from the much simpler NSW approximation.

It is rather evident from looking at the flow in Figure 12 that on a steep slope the large horizontal velocities are closely associated with vertical velocities of the same order of magnitude. Therefore, vertical accelerations cannot be neglected. That implies nonhydrostatic pressure which will feed back and create horizontal velocities that are not uniform over depth. The pressure variation along the slope has been computed and divided by the hydrostatic pressure corresponding to the instantaneous water level vertically above the considered point at the slope. Results show this pressure ratio deviates quite appreciably from +1 (corresponding to an hydrostatic pressure as assumed in the NSW equations). In the runup phase the ratio stays within 0.7 and 1.1. During the rush-down, however, it varies between 0.6 and 1.9. The horizontal velocity profiles along verticals can be inferred from Figure 12. This leads to diagrams such as in Figure 13 where it appears that the variation is almost invariably close to being linear with a nearly constant absolute shear.

The comparison with the NSW on a steep slope is further studied in Svendsen & Grilli 1989 [33] and in the next Section for the case of a gentle slope.

5 Interaction of a solitary wave with a gentle slope

5.1 Computation of the non-breaking runup of solitary waves

The problem of the interaction of solitary waves with a gentle slope has been studied in detail by Synolakis 1987 [35] (SY). By solving the Shallow Water equations, he developped asymptotic results for the maximum runup. Both linear and nonlinear theories led to the same *runup law* $\frac{\mathcal{R}}{d} = 2.831(\cot\beta)^{\frac{1}{2}}(\frac{H}{d})^{\frac{5}{4}}$, with $\mathcal{R}$ the maximum runup, and β the slope (this expression is only valid for $\frac{H}{d} \gg \frac{H_l}{d} = (0.288\tan\beta)^2$ where H_l refers to a lower bound for the wave). SY compared the *runup law* with his experimental results and with those of Hall & Watts' 1953 [18] (H&W) and pointed out that, in many studies, runup data have been analyzed without making a distinction between breaking and non-breaking solitary waves. That distinction is essential mainly for gentle slopes where most of the data refer to breaking waves. Hence SY used a criterion of breaking during backwash, developped by Pedersen & Gjevik 1983 [28] (from simplified analytic solutions) : $\frac{H}{d} \geq \frac{H_b}{d} = 0.479(\cot\beta)^{-\frac{10}{9}}$, to sort out the non-breaking runups in the above refered experiments, which were then compared with his theoretical predictions. The agreement was good in case of gentle slopes ($\beta = 2.88°$) but deteriorated when the steepness of the slope increased ($\beta \geq 45°$). By determining the conditions where the surface slope becomes infinite (his method breaks down soon after such situations), SY finally derived a criterion of breaking during the runup $\frac{H}{d} \geq \frac{H_m}{d} = 0.818(\cot\beta)^{-\frac{10}{9}} = 1.708\frac{H_b}{d}$.

A comparison between these analytical results, our BEM results and the experimental results of LVN, H&W and SY, is presented in Table 4. Our computations are performed in a 10m long and 0.3m deep numerical wavetank. The total discretization is N_Γ=158 (all but the 2.88° slope) to 190 (2.88° slope) nodes, with 101 nodes or 50 quasi-spline elements located on the free surface. Quadratic elements are used on the rest of the boundary. The time steps are Δt= .015 to .030s. The CPU time per time step is 1.17s to 1.71s on an IBM 3090/300.

Table 4 shows that on a 2.88° slope and for the smaller wave ($\frac{H}{d}$=0.019), SY's *runup law* predicts a runup 16% higher than his experimental result (which is here taken equal to the average of his 2 experiments for this wave : $\frac{\mathcal{R}}{d}$=0.078, 0.076 for d=0.3097, 0.3106m) whereas our solution is only 5% higher. Although it did not break in the experiments, the second wave ($\frac{H}{d}$=0.040) is larger than $\frac{H_m}{d}$ (equal to 0.029) and is indeed found to break during runup in both SY' and our results.

On a 15° slope and for the smaller wave ($\frac{H}{d}$=0.100), SY' *runup law* gives a runup in very good agreement (less than 1%) with our fully nonlinear solution. For the larger wave ($\frac{H}{d}$= 0.200), the discrepancy with our results is of 12%. Our results, agree with the experiments of H&W within 10% for both waves and those of SY within 10% and 22% for the two tested waves respectively. Notice that the second wave is greater than the limit of breaking during backwash estimated for this slope ($\frac{H_b}{d}$= 0.111) and is indeed found to break during the rundown in our computations. Notice, also, that Kim, *et al.* 1983 computed runups on a 15° slope (by a fairly low order BEM) for the same two waves as in Table 4 and found $\frac{\mathcal{R}_m}{d}$=0.308 and 0.766 for each of the waves respectively.

On a 45° slope, the discrepancy between SY' *runup law* and our results is of the order of 19%, whereas our results agree with the experiments of LVN within less than 3%. On a 70° slope, our runup results ag
with the *runup law* is not rele
is far too large ($\frac{H_l}{d}$ =0.617). If
SY) is used for the 45° and 70°
communication). This reduces
8% and 7% for the two slopes

Thus, the best prediction
experimental results within 7
In most of the cases our resul
10%). Although the number of
the experimental results can t
dispersive effects and friction.
but are neglected in the SW e
a *steep slope*, dispersive effect
velocities and accelerations bec
and 4.6). On a smooth steep
small importance. Only at the
expected (this problem was stu
show that our solution agrees
the higher discrepancy of the S
effects of vertical accelerations.
small. Dispersive effects, howev
also becomes important since l
effects should account for the 1
friction should mostly be respon
an *intermediate slope*, all three
only friction our solution. Thu
on a gentle slope whereas the
some 5% larger than that. This
H&W experiments. All this sh
more slopes.

5.2 Shoaling and breaki

As seen above, even small soli
can also be addressed with ou
simulated in the same numerica
β = 2.88° (slope 1:20), startin
varying time steps Δt = 0.0075
Goring's method of solit
$\frac{H}{d}$ = 0.794, greater than the wa
[36]). This wave almost stabili
Such a wave, however, was found
The shape of this highly
solitary wave (Figure 14). It s

70° slope, our runup results agree with the experiments within less than 4%. A comparison with the *runup law* is not relevant in this case, since the validity criterion of SY' solution is far too large ($\frac{H_i}{d}$ =0.617). If the full integral equation derived by SY (equation (3.3) in SY) is used for the 45° and 70° slopes, one gets the results named $\frac{R'}{d}$ in Table 4 (personal communication). This reduces the maximum discrepancy with the experimental results to 8% and 7% for the two slopes respectively.

Thus, the best predictions of solitary wave runups by the SW theory agree with the experimental results within 7 to 22% on 2.88° to 70° slopes (for the data in Table 4). In most of the cases our results are significantly closer to the experimental results (3 to 10%). Although the number of results available in Table 4 is limited, the discrepancies with the experimental results can tentatively be interpreted in terms of vertical accelerations, dispersive effects and friction. The two first effects are present in a fully nonlinear solution, but are neglected in the SW equation whereas friction is neglected in both solutions. On a *steep slope*, dispersive effects are negligible (small propagation distance), but vertical velocities and accelerations become important for the higher waves (as seen in Section 4.5 and 4.6). On a smooth steep slope, the influence of friction must be expected to be of small importance. Only at the uppermost tip of the runup, would some frictional effects be expected (this problem was studied by Packwood & Peregrine 1981 [27]). Results indeed show that our solution agrees with experiments within 4% (for 45° and 70° slopes). Thus, the higher discrepancy of the SW solution (8%) in this case should mostly be related to the effects of vertical accelerations. On a *gentle slope* the vertical velocities and accelerations are small. Dispersive effects, however, become important mainly for the higher waves. Friction also becomes important since longer distances of propagation are considered. Both of these effects should account for the 16% discrepancy of the SW solution on a 2.88° slope, whereas friction should mostly be responsible for the 5% discrepancy of our solution in this case. On an *intermediate slope*, all three effects should influence concurrently the SW solution, and only friction our solution. Thus one would expect discrepancies similar to those obtained on a gentle slope whereas the discrepancies obtained in both solutions on a 15° slope are some 5% larger than that. This could be due to a more important friction in the rather old H&W experiments. All this should anyway be investigated further with more waves and more slopes.

5.2 Shoaling and breaking of a solitary wave

As seen above, even small solitary waves break on a gentle slope. This kind of problem can also be addressed with our model. Shoaling and breaking of a high solitary wave is simulated in the same numerical wavetank as above, for the case of a gentle slope of angle β = 2.88° (slope 1:20), starting at x=4m. The computational data are as above with varying time steps Δt = 0.0075s to 0.00125s.

Goring's method of solitary wave generation is again used and creates a wave of $\frac{H}{d}$ = 0.794, greater than the wave of maximum energy ($\frac{H}{d} \simeq 0.78$, see Tanaka, *et al.* 1987 [36]). This wave almost stabilizes in the numerical wavetank after propagating over 10d. Such a wave, however, was found by Tanaka *et al.* to be unstable in a long term propagation.

The shape of this highly nonlinear wave is, as expected, rather far from a perfect solitary wave (Figure 14). It sheds a strong tail of disturbances as it propagates in the

β	$\frac{H_b}{d}$	$\frac{R_{up}}{d}$	$\frac{R_{up}}{d}$	$\frac{H_b}{d}$	$\frac{R}{d}$	$\frac{H_l}{d}$	$\frac{R'}{d}$
70°	0.259	0.580	0.558	1.472	0.316	0.617	0.524
70°	0.437	1.062	1.071	1.472	0.607	0.617	1.142
45°	0.269	0.674	0.672	0.479	0.546	0.083	0.644
45°	0.457	1.257	1.294	0.479	1.064	0.083	1.194
15°	0.100	0.310	0.281	0.111	0.308	0.006	(n.a.)
15°	0.200	0.654	0.599	0.111	0.732	0.006	(n.a.)
2.88°	0.019	0.081	0.077	0.017	0.089	0.000	(n.a.)
2.88°	0.040	(—)	0.156	0.017	0.226	0.000	(n.a.)

Table 4: Runup on a slope β : The $\frac{R_{up}}{d}$ are the BEM results. The $\frac{R_{up}}{d}$ are the experimental results from Losada, *et al.* 1986 (45° and 70°), from Hall & Watts 1953 (15°) and from Synolakis 1987 (2.88°). $\frac{R}{d}$ is the asymptotic *runup law* from Synolakis 1987 and $\frac{R'}{d}$ is the corresponding full expression. $\frac{H_b}{d}$ is the criterion of breaking during backwash from Pedersen & Gjevik 1983, and $\frac{H_l}{d}$ is the validity limit of Synolakis' *runup law*. (—) means there was breaking during the runup.

tank, and exhibits low scale modulations close to its tip. After reaching the slope (x=4m) the wave (surprisingly) slightly decreases in maximum height over the next 2m. Then, it starts shoaling and eventually breaks around $x = 6.95$m.

Figures 15a and 15b show the breaking process itself. Unlike with periodic waves, the breaking is very local and limited to a small jet at the tip of the wave. Tanaka *et al.* 1987 [36] found a somewhat similar breaking pattern in their computation of the instability of solitary waves over a constant depth.

6 Conclusions

The two-dimensional computations described here have been made with a version of the Boundary Integral Equation Method which does not apply complex variables and does not assume the waves are periodic in space. This method can also be used, as it is, for any kind of bottom geometry. It turns out that sawtooth instability does not occur (even after more than 1000 time steps), and that both energy and volume inside the computational region are controled sufficiently well to not making it necessary to carry out artificial adjustments during the computations as has been necessary in e.g. some of the computations reported by Dold & Peregrine 1984 [7].

Although the method has not yet been developed to its full capacity the results show that phenomena such as generation, long term propagation, breaking and runup on steep and gentle slopes, of large amplitude waves can accurately be predicted by this method. And because of the accuracy of the computations the method can also be used to analyze flow properties such as velocity and pressure fields that could not easily be measured during experiments in a physical wavetank.

The maximum runup of solitary waves on 2.88° to 90° slopes is shown to agree well

with experimental or other fu
elevations on a steep slope wi
even for the small scale oscill
pressure during reflection of a
discrepancies with the hypothe
non-hydrostatic pressure). Th
tant discrepancies with the exp
steep slopes. This is tentativ
effects (both neglected in the S
wave on a 1:20 slope shows th
the wave.

A Generation of a

In a wave of permanent form,

$$\int_{-d}^{\eta} u \, dz = c_a \eta + Q_s + U$$

where c_a is the propagation sp
wave elevation above the still
wave period, and U_c, the speed
wave trough level.

In a solitary wave with
simply reduces to $c\eta$ where c
becomes the simpler expression
a piston wavemaker to generat
the wavemaker. Since the pist
(5) reduces to,

$$u_p(d+\eta) = c\eta$$

which means that a required η

$$u_p(t) = \frac{c\eta}{d+\eta}$$

This corresponds to a piston m

$$x_p(t) = \int_0^t \frac{c\eta}{d+\eta} \, d\tau$$

To generate a solitary wave pro

$$\eta(x,t) = H \operatorname{sech}^2[\tfrac{\kappa}{d}(x - c$$

$$c = \sqrt{g(d+H)}$$

$$\kappa = \sqrt{\frac{3H}{4d}}$$

with experimental or other fully nonlinear results. Comparison of predicted free surface elevations on a steep slope with detailed experimental results shows a good agreement, even for the small scale oscillations behind the wave. The analysis of the velocity and pressure during reflection of a high solitary wave from a 45° slope shows some important discrepancies with the hypothesis and predictions of the SWE (important vertical velocity, non-hydrostatic pressure). The runups computed with the SWE also exhibit more important discrepancies with the experimental results than with our method, on both gentle and steep slopes. This is tentatively interpreted in terms of vertical acceleration, dispersive effects (both neglected in the SWE) and friction. Computation of the breaking of a solitary wave on a 1:20 slope shows that the overturning is limited to a small region at the tip of the wave.

A Generation of a solitary wave by a piston wavemaker

In a wave of permanent form, we have at any instant (Svendsen & Justesen [34]),

$$\int_{-d}^{\eta} u \ \mathrm{d}z = c_a \eta + Q_s + U_c d \tag{5}$$

where c_a is the propagation speed of the wave in a fixed frame of reference, $\eta(x,t)$ is the wave elevation above the still water level, Q_s is the nonlinear mass flux averaged over a wave period, and U_c, the speed of the current defined as the averaged particle velocity below wave trough level.

In a solitary wave with an infinitely long wave period, the right hand side of (5) simply reduces to $c\eta$ where c is the speed of the wave relative to the water, so that (5) becomes the simpler expression used by Goring [11] for determining the motion required by a piston wavemaker to generate a specified water surface elevation immediately in front of the wavemaker. Since the piston motion creates a depth uniform horizontal velocity $u_p(t)$ (5) reduces to,

$$u_p(d+\eta) = c\eta \tag{6}$$

which means that a required η can be generated by a piston velocity,

$$u_p(t) = \frac{c\eta}{d+\eta} \tag{7}$$

This corresponds to a piston motion $x_p(t)$ given by,

$$x_p(t) = \int_0^t \frac{c\eta}{d+\eta} \ \mathrm{d}\tau \tag{8}$$

To generate a solitary wave profile of amplitude H in water of constant depth d with,

$$\eta(x,t) = H\mathrm{sech}^2[\frac{\kappa}{d}(x-ct)] \tag{9}$$

$$c = \sqrt{g(d+H)} \tag{10}$$

$$\kappa = \sqrt{\frac{3H}{4d}} \tag{11}$$

(9)-(11) are substituted into (8) with $x = x_p(t)$ required throughout the integration in order to account for the finite amplitude of the piston. Notice that most wave maker theories describe the solution to the problem : What is the wave motion generated by a specified paddle motion ? It may be interesting to notice that the procedure described above is the only one (known to the authors) for solving the "inverse" wave generation problem : How do we move the wavemaker to generate a wave of a specified (arbitrary) form.

Since a solitary wave profile like (9) extends to infinity in both directions, Goring introduced a way of estimating the importance of the significant horizontal extension of the wave by defining an apparent wavelength 2λ which represents the part of the wave where $\eta > 0.001H$, with $\frac{\lambda}{d} = \frac{3.8}{\kappa}$ and $3.8 = \text{arcosh}[(\frac{1}{.001})^{\frac{1}{2}}]$.

The wave generation by the wavemaker starts at $t = 0$ with the begining of the solitary wave profile considered as significant, i.e. for $x = \lambda$. Therefore, in the wave formula (9), we set $x = x_p + \lambda$ and, by integrating (8), we get,

$$x_p(t) = \frac{H}{\kappa}[\tanh\frac{\kappa}{d}(ct - x_p - \lambda) + \tanh\frac{\kappa}{d}\lambda] \tag{12}$$

This formula, implicit in x_p, is solved for any given t by Newton iterations. Then $u_p(t)$ is computed by (7) for $\eta(x_p, t)$ and, eventually, $\frac{\partial u_p(t)}{\partial t}$ is found by derivation of (7). Hence, the boundary conditions can be defined on the wavemaker.

References

[1] Brorsen, M. & Larsen, J. Source Generation of Nonlinear Gravity Waves with the Boundary Integral Method. *Coastal Engineering* **11**, 93-113, 1987.

[2] Byatt-Smith, J.G.B. The Reflection of a Solitary Wave by a Vertical Wall. *J. Fluid Mech.* **197**, 503-521, 1988.

[3] Camfield, F.E. & Street, R.L. An Investigation of the Deformation and Breaking of Solitary Waves. *Dept. of Civil Engng., Stanford University, Technical Report No.* **81**, 1967.

[4] Carrier, G.F. Gravity Waves on Water of Variable Depth. *J. Fluid Mech.* **24** (4), 641-659, 1966.

[5] Carrier, G.F. & Greenspan, H.P. Water Waves of Finite Amplitude on a Sloping Beach. *J. Fluid Mech.* **4** (1), 97-110, 1958.

[6] Cointe, R., Molin, B. & Nays, P. Nonlinear and Second-Order Transient Waves in a Rectangular Tank. In *Proc. 6th Intl. Conf. on Behavior of Off-shore Structures, Delft (B.O.S.S.)*, 1988.

[7] Dold, J.W. & Peregrine, D.H. Steep Unsteady Water Waves : An Efficient Computational Scheme. In *Proc. 19th Intl. Conf. on Coastal Engineering, Houston, USA*, pp. 955-967, 1984.

[8] Dommermuth, D.G. & Yue, D.K.P. Numerical Simulation of Nonlinear Axisymmetric Flows with a Free Surface. *J. Fluid Mech.* **178**, 195-219, 1987.

[9] Fenton, J.D. & Rienecker, M.M. A Fourier Method for Solving Nonlinear Water-Wave Problems : Application to Solitary-Wave Interactions. *J. Fluid Mech.* **118**, 411-443, 1982.

[10] Gardner, C.S., Greene, J.M
Korteweg-de Vries Equation

[11] Goring D.G. Tsunamis - T
Laboratory of Hydraulics a
Report No. **KH-R-38**, 19

[12] Greenhow, M. & Lin, W.M
Generated by Wedge Entry
Numerical Ship Hydrody., *W*

[13] Greenhow, M. & Lin, W.M
in Two Dimensions. *MARI*
1986.

[14] Grilli, S., Skourup, J. & Sv
A Step Toward the Numeri
Boundary Elements, Southa
Computational Mechanics P

[15] Grilli, S., Skourup, J. & Sv
Nonlinear Water Waves. *En*

[16] Grilli, S. & Svendsen, I.A.
Improvements to the Num
on Boundary Elements, Co
ics Publication. Springer Ve

[17] Grilli, S. & Svendsen, I.A.
Maritime Structures. To app
bridge, Massachusetts, USA
Berlin, 1989b.

[18] Hall, J.V. & Watts, J.W.
Waves on Impermeable Slo
Tech. Memo. No. **33**, 14 p

[19] Hammack, J.L. & Segur, H.
2. Comparison with Experi

[20] Kim, S.K., Liu, P.L.-F. &
Solitary Wave Generation P
1983.

[21] Kravtchenko, J. Remarques
par un batteur. In *Proc. 5t*

[22] Lin, W.M., Newman, J.N.
In *Proc. 15th Intl. Symp. o*

[23] Longuet-Higgins, M.S. & C
Water - I. A Numerical Me
1976.

[24] Losada, M.A., Vidal, C. & M
por Perfiles de Playa en Ba
Costas Programa de Clima
1986.

[10] Gardner, C.S., Greene, J.M., Kruskal, M.D. & Miura, R.M. Method for Solving the Korteweg-de Vries Equation. *Physical Revue Letters* **19**, (19), 1095-1097, 1967.

[11] Goring D.G. Tsunamis - The Propagation of Long Waves onto a Shelf. *W.M. Keck Laboratory of Hydraulics and Water Ressources, California Institute of Technology, Report No.* **KH-R-38**, 1978.

[12] Greenhow, M. & Lin, W.M. Numerical Simulation of Nonlinear Free Surface Flows Generated by Wedge Entry and Wave-maker Motions. In *Proc. 4th Intl. Conf. on Numerical Ship Hydrody., Washington, USA,* 1985.

[13] Greenhow, M. & Lin, W.M. The Interaction of Nonlinear Free Surfaces and Bodies in Two Dimensions. *MARINTEK, Report No.* **OR/53/530030.12/01/86**, 36 pps, 1986.

[14] Grilli, S., Skourup, J. & Svendsen, I.A. The Modelling of Highly Nonlinear Waves : A Step Toward the Numerical Wave Tank. Invited paper in *Proc. 10th Intl. Conf. on Boundary Elements, Southampton, England,* Vol. 1 (ed. C.A. Brebbia), pp. 549-564. Computational Mechanics Publication. Springer Verlag, Berlin, 1988.

[15] Grilli, S., Skourup, J. & Svendsen, I.A. An Efficient Boundary Element Method for Nonlinear Water Waves. *Engineering Analysis with Boundary Elements* **6** (2), 1989.

[16] Grilli, S. & Svendsen, I.A. The Modelling of Highly Nonlinear Waves. Part 2 : Some Improvements to the Numerical Wave Tank. To appear in *Proc. 11th Intl. Conf. on Boundary Elements, Cambridge, Massachusetts, USA*. Computational Mechanics Publication. Springer Verlag, Berlin, 1989a.

[17] Grilli, S. & Svendsen, I.A. The Modelling of Nonlinear Water Wave Interaction with Maritime Structures. To appear in *Proc. 11th Intl. Conf. on Boundary Elements, Cambridge, Massachusetts, USA*. Computational Mechanics Publication. Springer Verlag, Berlin, 1989b.

[18] Hall, J.V. & Watts, J.W. Laboratory Investigation of the Vertical Rise of Solitary Waves on Impermeable Slopes. *Beach Erosion Board, US Army Corps of Engineer, Tech. Memo. No.* **33**, 14 pp, 1953.

[19] Hammack, J.L. & Segur, H. The Korteweg-de Vries Equation and Water Waves. Part 2. Comparison with Experiments. *J. Fluid Mech.* **65** (2), 289-314, 1974.

[20] Kim, S.K., Liu, P.L.-F. & Liggett, J.A. Boundary integral Equation Solutions for Solitary Wave Generation Propagation and Run-up. *Coastal Engineering* **7**, 299-317, 1983.

[21] Kravtchenko, J. Remarques sur le calcul des amplitudes de la houle lineaire engendrée par un batteur. In *Proc. 5th Intl. Conf. on Coastal Engineering,* pp. 50-61, 1954.

[22] Lin, W.M., Newman, J.N. & Yue, D.K. Nonlinear Forced Motion of Floating Bodies. In *Proc. 15th Intl. Symp. on Naval Hydrody., Hamburg, Germany,* 1984.

[23] Longuet-Higgins, M.S. & Cokelet, E.D. The Deformation of Steep Surface Waves on Water - I. A Numerical Method of Computation. *Proc. R. Soc. Lond.* **A350**, 1-26, 1976.

[24] Losada, M.A., Vidal, C. & Nunez, J. Sobre El Comportamiento de Ondas Propagádose por Perfiles de Playa en Barra y Diques Sumergidos. *Dirección General de Puertos y Costas Programa de Clima Maritimo. Universidad de Cantábria. Publicación No.* **16**, 1986.

[25] Mirie R.M. & Su C.H. Collisions Between Two Solitary Waves. Part 2. A Numerical Study. *J. Fluid Mech.* **115**, 475-492, 1982.

[26] Nagai, S. Pressures of Standing Waves on Vertical walls *J. Waterways, Harbors Div. ASCE* **95**, 53-76, 1969.

[27] Packwood, A.R. & Peregrine, D.H. Surf and Runup on Beaches : Models of Viscous Effects. *School of Mathematics, University of Bristol, Report No.* AM-81-07, 1981.

[28] Pedersen, G. & Gjevik, B. Run-up of Solitary Waves *J. Fluid Mech.* **135**, 283-299, 1983.

[29] Peregrine, D.H. Flow Due to a Vertical Plate Moving in a Channel. *Unpublished Notes*, 1972.

[30] Roberts, A.J. Transient Free-Surface Flows Generated by a Moving Vertical Plate. *Q.J. Mech. Appl. Math.* **40** (1), 129-158, 1987.

[31] Su, C.H. & Gardner, C.S. Korteweg-de Vries Equation and Generalizations. III. Derivation of the Korteweg-de Vries Equation and Burgers Equation. *J. Math. Phys.* **10** 536-539, 1969.

[32] Su, C.H. & Mirie, R.M. On Head-on Collisions between two Solitary Waves. *J. Fluid Mech.* **98** 509-525, 1980.

[33] Svendsen, I.A. & Grilli, S. Nonlinear Waves on Slopes. To appear in *J. Coastal Res.*, 1989.

[34] Svendsen, I.A. & Justesen, P. Forces on Slender Cylinders from Very High and Spilling Breakers. In *Proc. Symp. on Description and Modelling of Directional Seas*, paper No. D-7, 16 pps. Technical University of Denmark, 1984.

[35] Synolakis, C.E. The Runup of Solitary Waves. *J. Fluid Mech.* **185**, 523-545, 1987.

[36] Tanaka, M., Dold, J.W., Lewy, M. & Peregrine, D.H. Instability and Breaking of a Solitary Wave. *J. Fluid Mech.* **185**, 235-248, 1987.

[37] Vinje, T. & Brevig, P. Numerical Simulation of Breaking Waves. *Adv. Water Ressources* **4**, 77-82, 1981.

[38] Yim, B. Numerical Solution for Two-Dimensional Wedge Slamming with a Nonlinear Free surface Condition. In *Proc. 4th Intl. Conf. on Numerical Ship Hydrody., Washington, USA*, 1985.

Figures

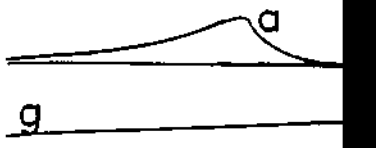

Fig. 1a: Sketch of a cross-secti
the gentle slope in front of the s
in shallow water and b a smalle

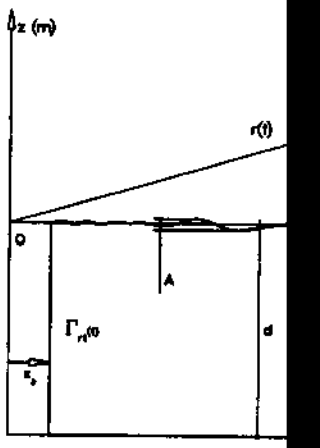

Fig. 1b: Sketch of the region us
parameters.

Figures

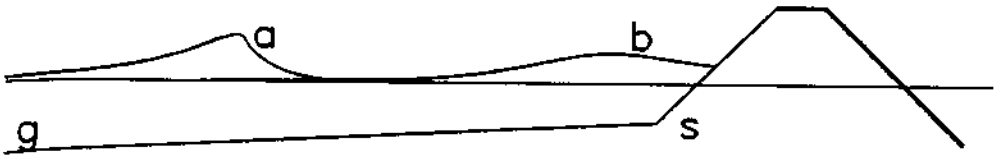

Fig. 1a: Sketch of a cross-section in a coastal area protected by a maritime structure. g is the gentle slope in front of the structure, s the steep structure slope, a a high wave breaking in shallow water and b a smaller wave runing-up on the structure.

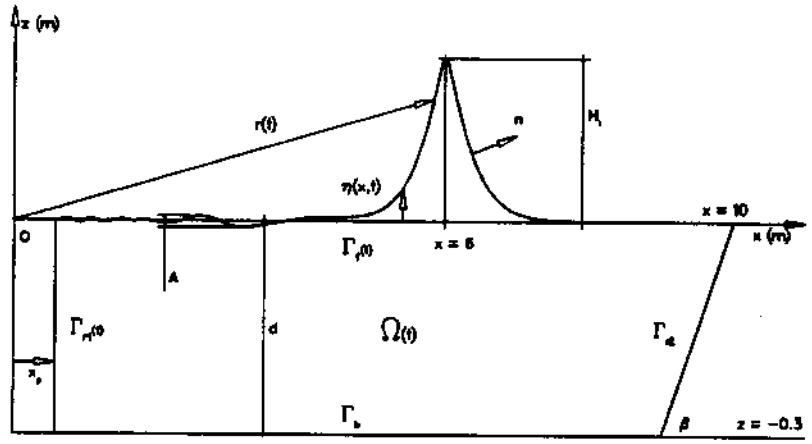

Fig. 1b: Sketch of the region used in the numerical computations. Definition of geometrical parameters.

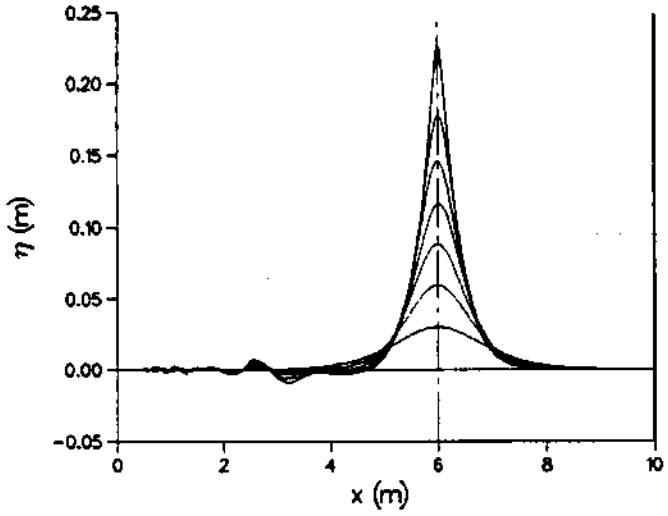

Fig. 2: Surface profile $\eta(x)$ for solitary waves of height $\frac{H}{d} = 0.1$ through 0.7. Each wave is shown at the moment the crest passes $x = 6$m (20 water depth d from the wave generator). The propagation times are : $\frac{H}{d} = 0.1$: 5.66s, 0.2 : 4.79s, 0.3 : 4.34s, 0.4 : 4.04s, 0.5 : 3.80s, 0.6 : 3.62s, 0.7 : 3.44s.

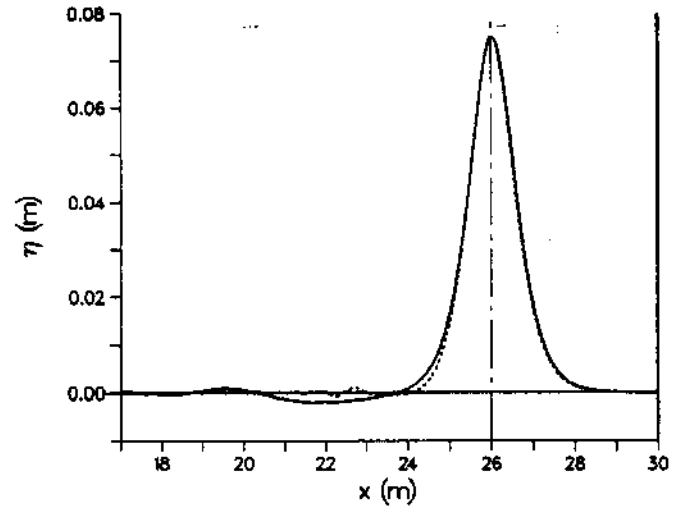

Fig. 3: Comparison between two solitary wave surface profiles generated at $x = 20$m (- - -) and $x = 0$m (——) respectively (i.e. after propagating 20 d and 86.6 d, d=0.30m). To be of the same height at $x = 26$m the two waves were generated with slightly different amplitude.

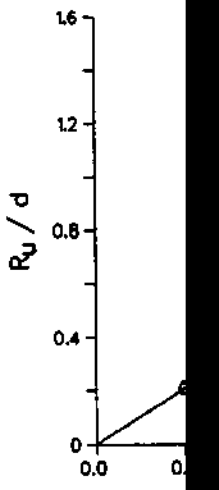

Fig. 4: Runup R_u for reflectio
$\frac{H}{d}$ for the wave 4m (13.3 d) in
order results, (□) Fenton & Ri
results.

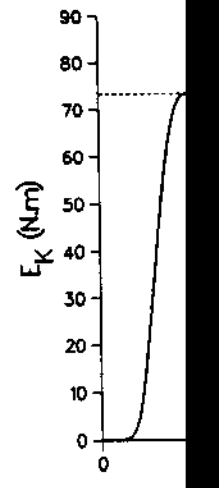

Fig. 5: Change in kinetic en
wall, for a wave of $\frac{H}{d}$=0.456.
minimum occurs slightly befo

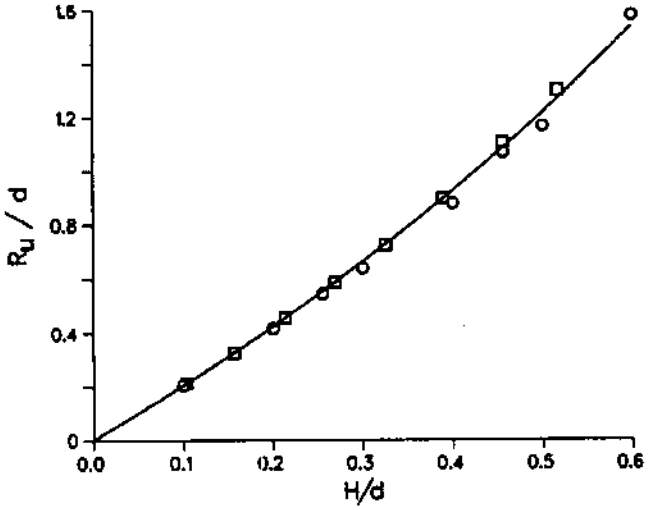

Fig. 4: Runup R_u for reflection of a solitary wave from a vertical wall versus the value of $\frac{H}{d}$ for the wave 4m (13.3 d) in front of the wall (as in Fig. 1). (——) Su & Mirie (1980) 3rd order results, (□) Fenton & Rienecker (1982) Fourier Method results and (o) present BEM results.

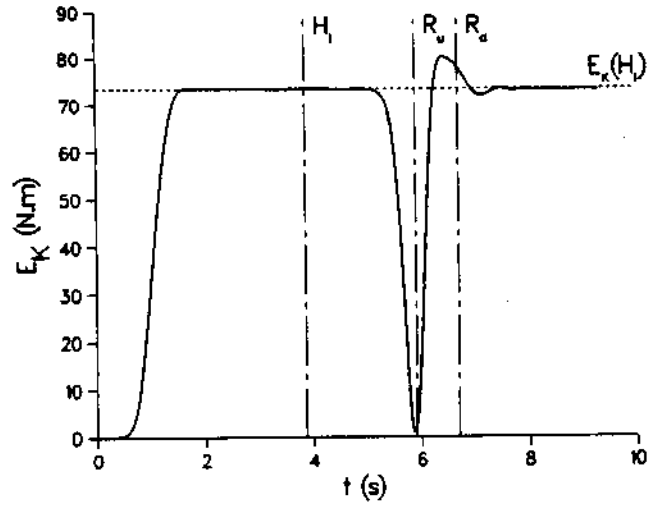

Fig. 5: Change in kinetic energy E_K during reflection of a solitary wave from a vertical wall, for a wave of $\frac{H}{d}$=0.456. Notice the kinetic energy never quite reaches zero, and the minimum occurs slightly before the instant of maximum runup.

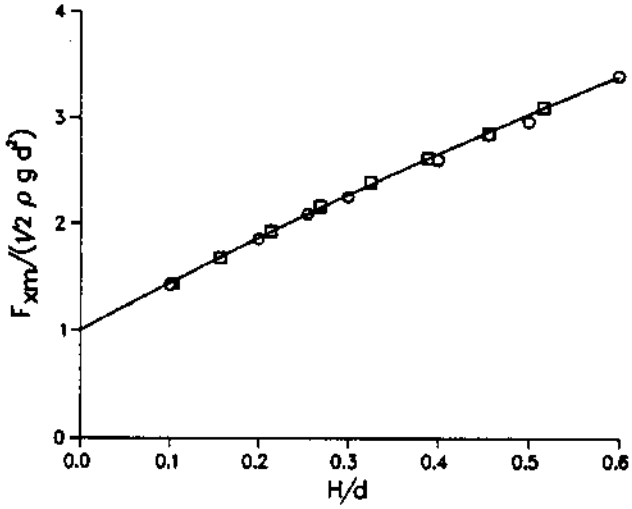

Fig. 6: Maximum horizontal pressure force F_{xm}, in dimensionless form, on a vertical wall during reflection of a solitary wave, as a function of $\frac{H}{d}$. Symbols are as in Fig. 5.

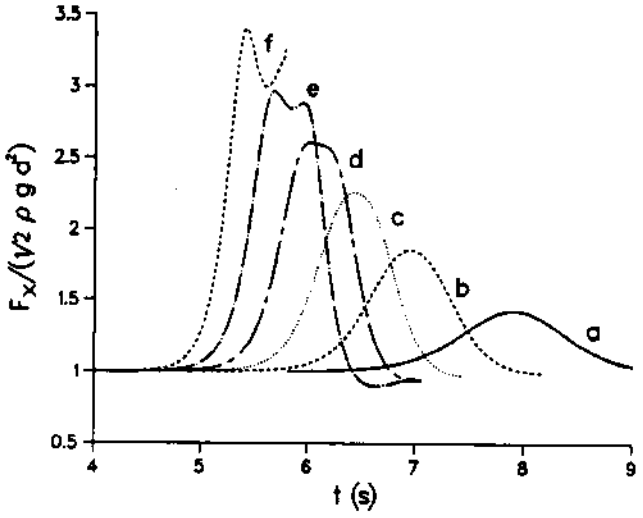

Fig. 7: Horizontal pressure force F_x, in dimensionless form, on a vertical wall during reflection of a solitary wave. $\frac{H}{d}$ = (a) : 0.1, (b) : 0.2, (c) : 0.3, (d) : 0.4, (e) : 0.5, (f) : 0.6.

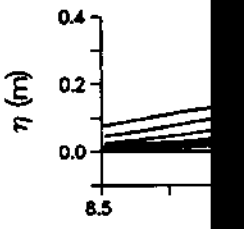

Fig. 8: Reflection of a solitar
maximum runup. Curves are

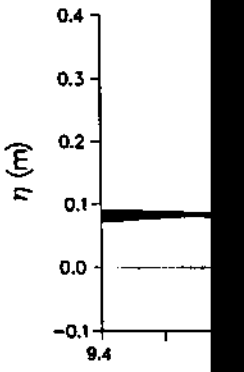

Fig. 9: Reflection of a solita
maximum runup, down to ba
6.5s and every 0.02s for t=6.5

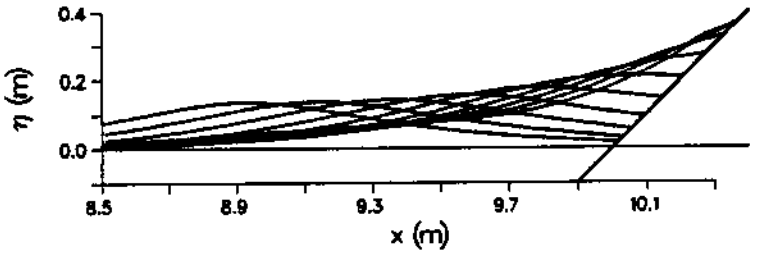

Fig. 8: Reflection of a solitary wave from a 45° slope, $\frac{H}{d}$= 0.457. Numerical results up to maximum runup. Curves are plotted every 0.1s for t=5.3 to 6.2s.

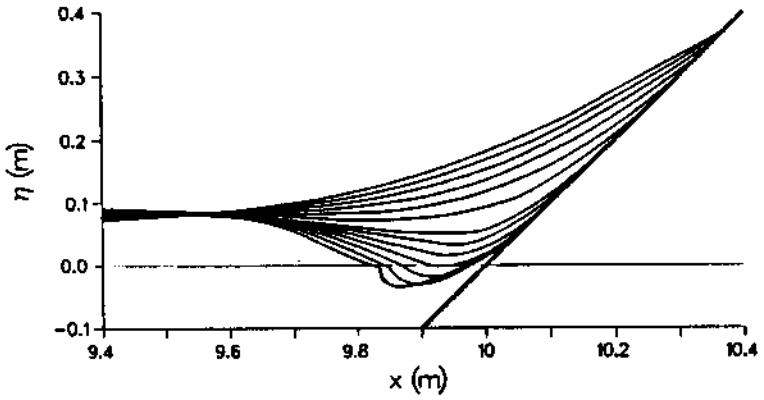

Fig. 9: Reflection of a solitary wave from a 45° slope, $\frac{H}{d}$= 0.457. Numerical results from maximum runup, down to backward breaking. Curves are plotted every 0.05s for t=6.2 to 6.5s and every 0.02s for t=6.50 to 6.64s.

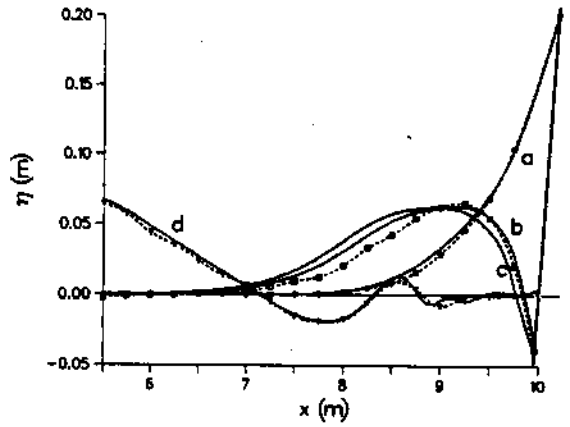

Fig. 10: Comparison between computations (——) and measurements (- - -) by Losada, et al. (1986) for reflection from a 45° slope, $\frac{H}{d}$= 0.269 with : (a) Instant of maximum runup (t = 6.77s in computations), (b) Instant of lowest position of water surface in experiments (t = 7.31s), (c) Instant of lowest surface position in computations (t = 7.38s in computations), (d) t = 9.08s.

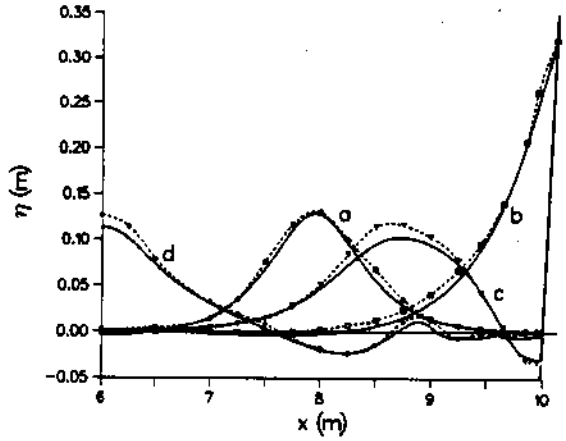

Fig. 11a: Same as Fig. 10 for a 70° slope, $\frac{H}{d}$= 0.437 with : (a) Wave profile somewhat before maximum runup (t = 4.88s), (b) Instant of maximum runup (t = 6.04s in computations), (c) Instant of lowest position of water surface in computations (t = 6.67s), (d) t = 7.97s.

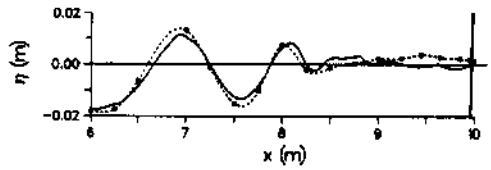

Fig. 11b: Same as Fig. 10 for a 70° slope, $\frac{H}{d}$= 0.437. Detail on the "Wave tail" profile at t = 9.48s

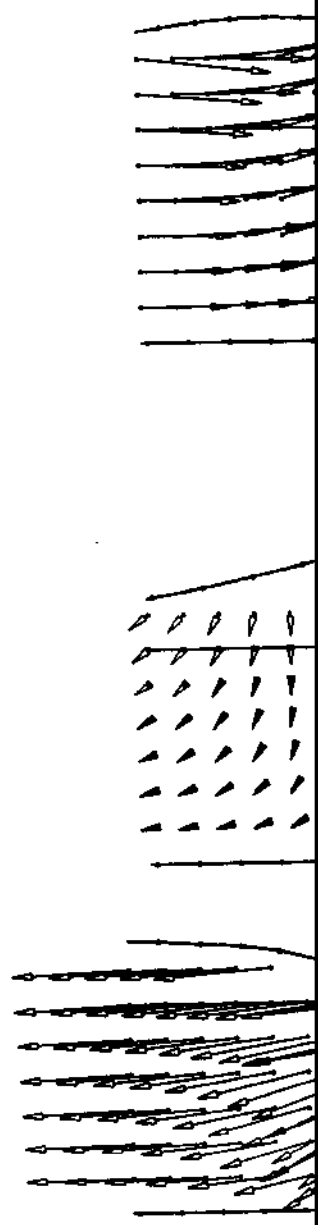

Fig. 12a-d: The internal ve
$\frac{H}{d}$= 0.457 on a 45° slope, a

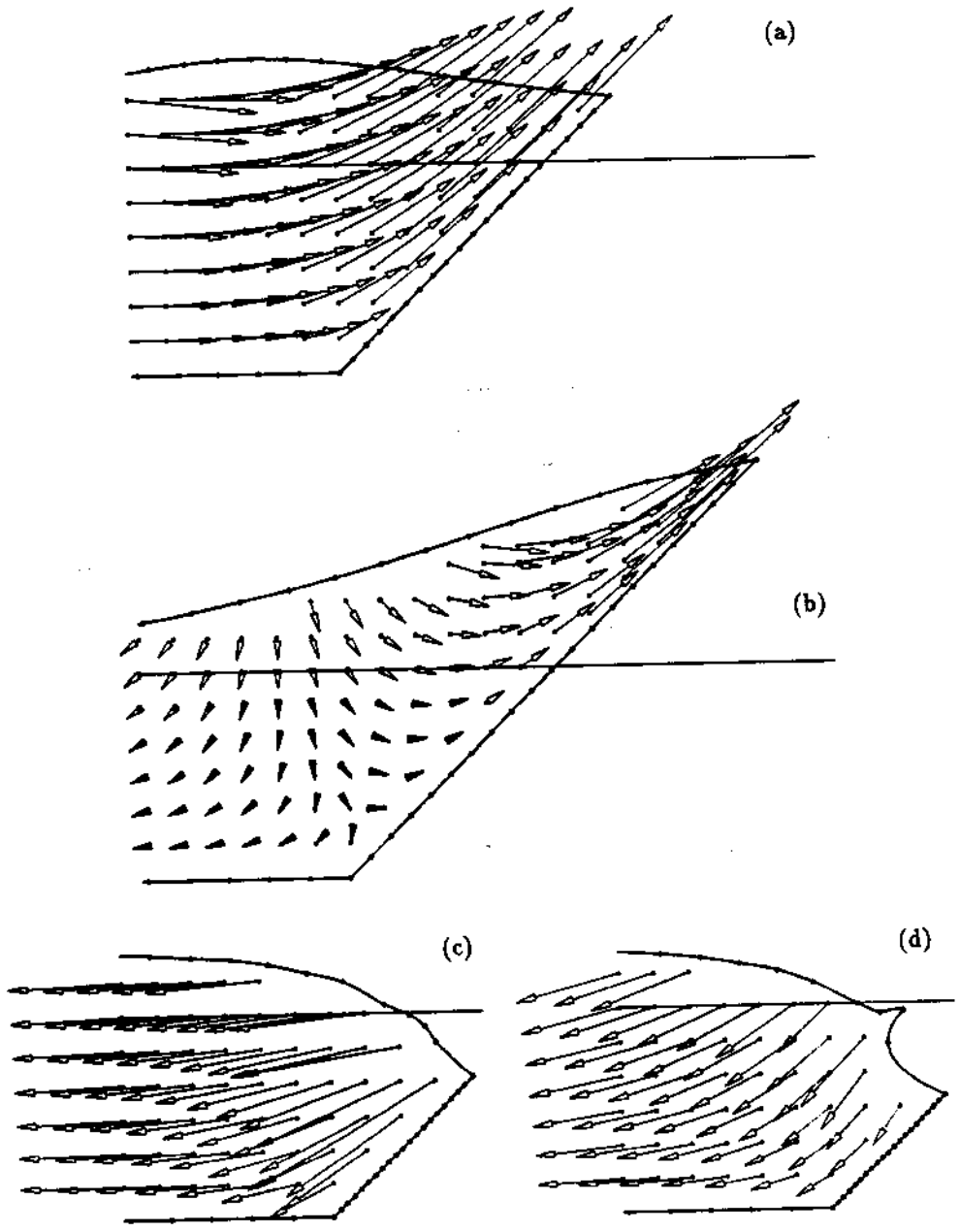

Fig. 12a-d: The internal velocity field during runup and rundown of a solitary wave with $\frac{H}{d} = 0.457$ on a 45° slope, at time (a) : 5.60s, (b) : 5.93s, (c) : 6.65s, (d) : 6.73s.

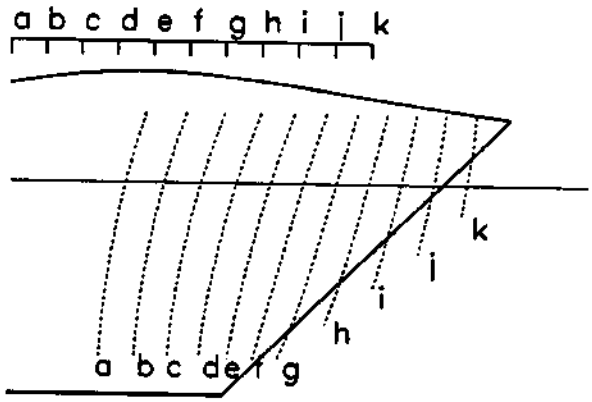

Fig 13 : (- - -) Envelopes of the horizontal velocity vectors of Fig. 12a. Vectors start at the positions of the upper letters and end on the corresponding curves.

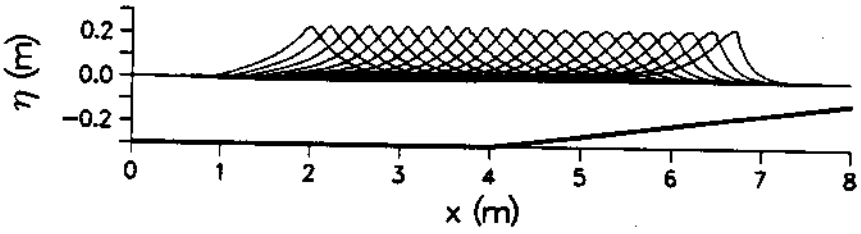

Fig. 14: Shoaling and breaking of a solitary wave of $\frac{H}{d}= 0.794$ on a 1:20 slope. Curves are plotted every 0.1s for t= 1.6 to 3.7s.

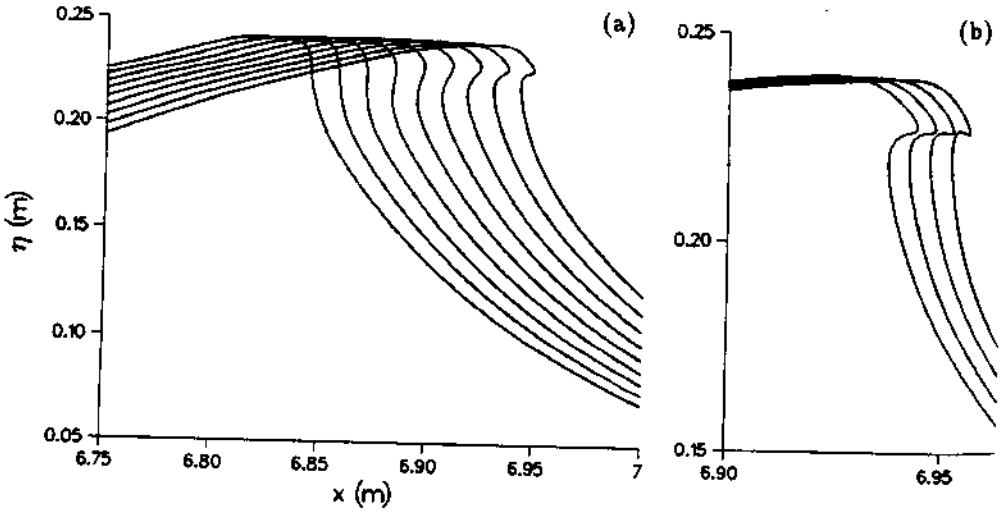

Fig. 15a-b: Details of the breaking of the same solitary wave as in Fig.14.

FIELD OBSERVATIONS OF WAVE-

R. L. SOULSBY
Hydraulics Reseai
Wallingford
Oxon OX10 8BA
UK

ABSTRACT. Field measurem
and wave-induced velocitie
wave-plus-current flow, wi
interaction. A technique
spectrum was developed to
turbulent fluctuations, wh
velocities. The wave boun
measuring height (10cm) an
current boundary layer, an
roughness. This caused bo
bed shear stress to increa
results have implications
dissipation, and forces o

1. INTRODUCTION

Over most of the continen
currents occur at the sea
interact nonlinearly near
taken into account in pra
transport or forces on su
approaches have been prop
structure of the combined
Bijker, 1967; Grant and M
1988; Myrhaug and Slaatte
qualitatively on a number
bed shear stress and the
differ markedly in their
1988). Field data to tes
notable exception of the
generally been made over
interpretation. To help
presented here of the ve
immobile rough bed.

A. Tørum and O. T. Gudmestad (eds.),